Communication

Controlled reduction of photobleaching in DNA origami – gold nanoparticle hybrids

Jesica Vanesa Pellegrotti, Guillermo P. Acuna, Anastasiya Puchkova, Phil Holzmeister, Andreas Gietl, Birka Lalkens, Fernando D Stefani, and Philip Tinnefeld

Nano Lett., **Just Accepted Manuscript** • Publication Date (Web): 01 Apr 2014

Controlled reduction of photobleaching in DNA origami – gold nanoparticle hybrids

Jesica V. Pellegrotti[1,2], Guillermo P. Acuna[3]*, Anastasiya Puchkova[3], Phil Holzmeister[3], Andreas Gietl[3], Birka Lalkens[3], Fernando D. Stefani[1,2]* and Philip Tinnefeld[3]

[1] Centro de Investigaciones en Bionanociencias (CIBION), Consejo Nacional de Investigaciones Científicas y Técnicas (CONICET), Godoy Cruz 2390, C1425FQD Buenos Aires, Argentina

[2] Departamento de Física, Facultad de Ciencias Exactas y Naturales, Universidad de Buenos Aires, Int. Güiraldes 2620, C1428EAH Ciudad de Buenos Aires, Argentina

[3]NanoBioSciences Group, Institute for Physical and Theoretical Chemistry, Technische Universität Braunschweig, Hans-Sommer- Strasse 10, 38106 Braunschweig, Germany.

*g.acuna@tu-bs.de, fernando.stefani@cibion.conicet.gov.ar

Abstract

The amount of information obtainable from a fluorescence-based measurement is limited by photobleaching: Irreversible photochemical reactions either render the molecules non-fluorescent or shift their absorption and/or emission spectra outside the working range. Photobleaching is evidenced as a decrease of fluorescence intensity with time, or in the case of single molecule measurements, as an abrupt, single-step interruption of the fluorescence emission which determines the end of the experiment. Reducing photobleaching is central for improving fluorescence (functional) imaging, single molecule tracking and fluorescence based biosensors and assays. In this single molecule study, we use DNA self-assembly to produce hybrid nanostructures containing individual fluorophores and gold nanoparticles at a controlled separation distance of 8.5 nm. By changing the nanoparticles size we are able to systematically increase the mean number of photons emitted by the fluorophores before photobleaching.

Keywords: DNA self-assembly, single-molecule, photobleaching, plasmonics, gold nanoparticle

As a key characteristic of a fluorophore, the photobleaching yield Q_b is in fact more important than the absorption cross-section or the quantum efficiency because it directly determines the total number of photons one can gather from a fluorescent molecule, and therefore the amount of information one can extract from the measurement. We will consider the simplest case where an excited fluorophore has only three possibilities: i) emitting a fluorescence photon with a given radiative decay rate k_r , ii) relaxing back to the ground-state without the emission of a photon, with a non-radiative decay rate k_{nr} , and iii) undergo photobleaching at a rate k_b . Under these conditions, the efficiencies of photon emission Q_r and photobleaching Q_b are given by

$$Q_r = \frac{k_r}{k_r+k_{nr}+k_b} , \qquad Q_b = \frac{k_b}{k_r+k_{nr}+k_b} . \qquad (1)$$

Generally, fluorophores do emit a considerable number of photons before photobleaching and k_b, being much smaller than $k_r + k_{nr}$, is neglected in calculations of Q_r. The total number of photons N emitted by the fluorophore before photobleaching is given by the ratio of efficiencies:

$$N = \frac{Q_r}{Q_b} = \frac{k_r}{k_b} . \qquad (2)$$

From equation (2) one directly sees that N is independent of k_{nr}, as first pointed out by Hirschfeld[1], and also independent of the excitation rate; i.e. N is independent of any plasmonic enhancement of the electric field at the fluorophore position. Equation (2) also shows the two possible pathways to reduce photobleaching: reducing k_b or enhancing k_r. Synthetic chemistry strategies aim to reduce the photobleaching rate k_b by modifying the ground and excited state energy landscapes of fluorophores. Indeed several families of fluorophores have been made more resistant to photobleaching by means of chemical modifications[2–4]. Also, in some situations k_b can be reduced by controlling the environment in order to protect the fluorophore against photobleaching reactions, like for example with oxygen scavenging solutions[5–9].

The alternative, physical approach to harvest more photons from fluorescent molecules is based on enhancing the radiative decay rate of the fluorophore k_r. As the molecule spends shorter times in the excited state before the emission of a photon, it can perform more excitation-emission cycles before undergoing photobleaching. The way to physically enhance k_r is based on Fermi's "golden rule":

$$k_r = \left[\frac{\langle i|H|f\rangle^2}{\hbar^2}\right]\rho(\nu) . \qquad (3)$$

The state $\langle i|$ corresponds to the excited molecule in the absence of any photon, $\langle f|$ is the final state of the relaxed molecule and a single photon, H is the molecule-field interaction Hamiltonian. The key factor in equation (3) is $\rho(\nu)$, the density of photon states at the emission frequency ν. A higher photonic mode density (PMD) of the right frequency and polarization facilitates a faster radiative decay of the excited fluorophore. Purcell was the first one to recognize that small metallic particles could enhance k_r at radiofrequencies[10]. At optical frequencies, the pioneering work by Drexhage[11] on fluorescent molecules near metallic surfaces clearly established that metallic structures supporting surface plasmons are ideal to produce strong modifications of the PMD. Meanwhile, the influence of the PMD on molecular fluorescence and phosphorescence has been extensively studied and understood in numerous plasmonic systems including thin films, colloidal nanoparticles and top-down fabricated structures [12–20].

Remarkably, most investigations on plasmonic enhancement of molecular fluorescence have focused on enhancing intensity and the emission directionality. In spite of its fundamental practical significance, the possibility of increasing photostability of fluorophores by means of an enhanced PMD has remained rather unexplored. Since the first theoretical prediction made by Enderlein[21] for a molecule near a plane metallic surface, a handful of experimental investigations have been reported. Reduced photobleaching was observed for fluorescent dyes in the vicinity of silver island films[22]. In a systematic study using monolayers of fluorophores in front of a thin gold film, evidence supporting Enderlein was found[23]. Recently, it was reported that fluorophores incorporated into gold nanoshells are considerably more resistant to photobleaching[24], and that single fluorophores adsorbed onto a silver nanoparticle dimer can emit a substantially larger number of photons before photobleaching[25]. However, none of these investigations constitutes a clear-cut experimental proof of the PMD mechanism, or offered control over the photostability. Here, we combine a highly precise bottom-up nano-fabrication using DNA self-assembly, time-resolved single molecule measurements, and 3D electromagnetic calculations, in order to produce a controlled reduction of photobleaching that can be fully ascribed to the local enhancement of the photonic mode density nearby gold nanoparticles.

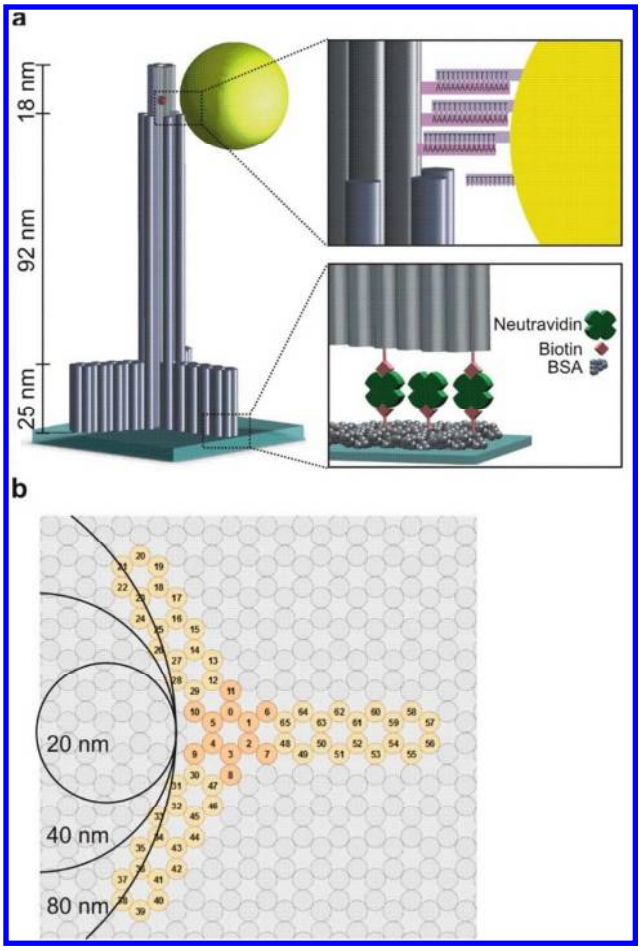

Figure 1. (a) Sketch of the DNA origami pillar (grey) labeled with a Cy5 dye (red) immobilized on a glass surface. Single AuNPs of different size can bind, via a set of oligonucleotide chains laterally, with its equator at the same height as the dye. (b) Upper view of the pillar structure showing the 66 helices that conform the main shaft (orange) and the base (yellow). The circles schematically show on scale the sizes of the AuNPs used.

DNA origami – fluorophore - AuNP hybrid nano-structures

Figure 1a depicts a sketch of the nano-structures used in our experiments. A new pillar-shaped DNA origami structure (in gray) is used as scaffold to incorporate a single Cy5 molecule (in red) and a single AuNP in controlled positions via DNA hybridization. The pillar structure is made of 66 DNA helices arranged in a vertical manner, an upper view is included in figure 1b. The main shaft is made of a twelve-helix-bundle (helices 0-11 in figure 1b). At the top of the structure, a six-helix-bundle (helices 0-5) protrudes over the last 18 nm. The structure is completed by three linear structures at the bottom with the remaining helices (12-65) forming the base. For distance estimation, we consider a distance of 0.34 nm between two adjacent base pairs and of 3 nm between two adjacent helices[26]. The Cy5 molecule is incorporated approximately at the center of the six-helix-bundle at a height of 122 nm. The pillar structures labeled with the Cy5 are immobilized on a previously functionalized glass surface using biotin-neutravidin[27] (figure 1a). Conditions are adjusted until a surface occupancy of about 1 structure per squared micrometer, suitable for single-molecule microscopy, is reached. Following immobilization, AuNPs surface functionalized with a Thiol-5'-15T-3' are added in solution. AuNPs of 20, 40 or 80 nm in diameter were used. The AuNPs bind to complimentary strands protruding from helices 4 and 5 at a height of 122 nm (figure 1a). This sequential binding approach avoids aggregation of multiple origami structures to the same AuNP[28]. Furthermore, by adjusting the concentration and incubating time of the AuNPs the yield of AuNP binding can be controlled in order to preserve a population of pillars without AuNPs for internal referencing. Based on the sample geometry, we estimate the distance between the dye and the AuNP surface to be 8.5 nm for every particle size.

Single-molecule fluorescence measurements

Fluorescence intensity and lifetime imaging was performed on a home-built sample-scanning confocal microscope. For excitation, a pulsed laser with circularly polarized light at 640 nm was employed. Fluorescence light was spectrally separated from the excitation by appropriate interference filters and detected using an avalanche photodiode and a time correlated single photon counting (TCSPC) module. In the measurements, we first obtained an image of a region of the sample and located the Cy5-labelled DNA structures. Then, we moved the sample sequentially in order to position, one at a time, each one of the detected DNA structures into the laser focus and measure the time-resolved fluorescence emission of its Cy5 label until photobleaching occurred. In order to assure that each transient corresponded to a single molecule, it was verified that photobleaching occurred in a single step, otherwise they were discarded. The procedure was repeated until about 250 single-molecule fluorescence emission transients were obtained from each sample. We analyzed each single-molecule transient in order to obtain its average fluorescence intensity (detected count rate), total number of detected photons and fluorescence lifetime. The total number of detected photons is in all cases a constant fraction of the total number of emitted photons due to the collection and detection efficiencies of our microscope. Hereafter, we use N to refer to the total number of detected photons. See Methods for further details.

Due to the controlled yield of AuNP binding to the DNA-origami scaffolds, each sample contained a fraction of structures without nanoparticles attached, which served as reference. The first experimental task is to identify these two populations and determine for each Cy5 molecule whether it was measured under the presence of a nearby AuNP or not. A fluorophore placed in the near field of a metallic particle is expected to experience a different excitation rate as well as modified decay rates[29]. We first analyzed the fluorescence lifetime of each Cy5 molecule measured. In all three samples the two populations of structures, with and without AuNPs bound, were easily identified by inspecting the lifetime distributions (figure 2, upper panels). The fluorophores of the reference populations presented an average fluorescence lifetime of about 1 ns, whereas the fluorophores

close to the AuNPs all presented a significantly shorter lifetime. Based on its fluorescence lifetime value, each single transient was classified as reference (no AuNP) or bound to a AuNP of the corresponding size.

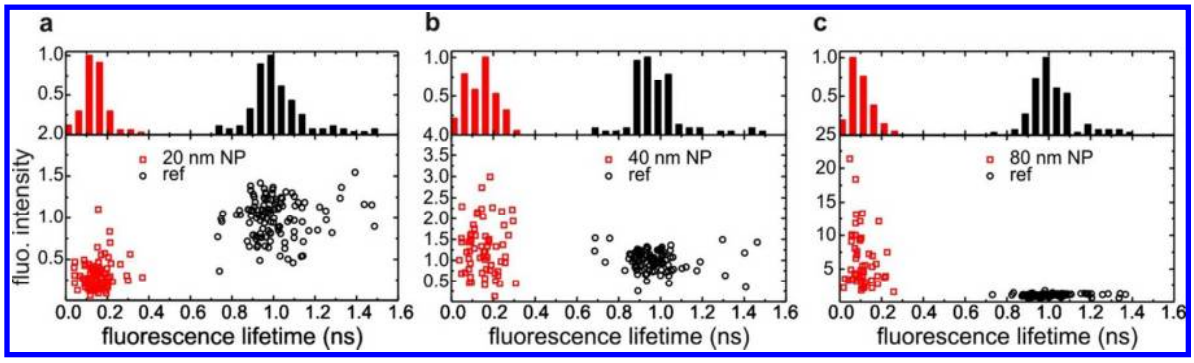

Figure 2. Upper panels: normalized frequency histograms of fluorescence lifetimes found in the samples of AuNPs with diameters of 20 (a), 40 (b) and 80 nm (c). In each sample, two populations are clearly visible. One with an average lifetime of about 1 ns corresponding to DNA-Cy5 without a AuNP bound (reference, black) and another one with much shorter fluorescence lifetime corresponding to DNA-Cy5 constructs with a AuNP attached (red). Lower panels: scatter plots of fluorescence intensity vs. lifetime. The values of fluorescence intensity are normalized to the average of the reference population.

The near field intensity produced by the AuNPs at the fluorophore position is also expected to be quite different for the AuNPs of 20, 40 and 80 nm. The average fluorescence intensity of each individual molecule was normalized to the average of the reference population of each sample (figure 2, lower panels). The reference populations in each sample presented similar fluorescence intensity distributions, whereas the populations of molecules near AuNPs showed different intensities depending on the nanoparticle size. When placed near the 20 nm AuNPs, the fluorophores emit on average with a lower intensity of about 30% of the reference value. In contrast, the 40 nm AuNPs cause a slight increase of the fluorescence intensity and finally, the presence of the 80 nm AuNPs produces a strong 3 to 20-fold increase of intensity in agreement with previous measurements[28]. The different fluorescence intensity distributions observed on the three samples clearly evidence a size dependent effect of the AuNPs. The distributions of fluorescence intensities are broadened by two sources of variation on the excitation rate. First, the distribution of binding orientations of the DNA pillars on the glass[30]. And second, for each nominal size of AuNPs, there is also a contribution from the distribution of nanoparticle size and shape[28,31]. In addition, changes in intensity cannot be uniquely ascribed to changes of the excitation rate because modifications of Q_r are expected too since AuNPs also produce modifications of k_r and k_{nr}.

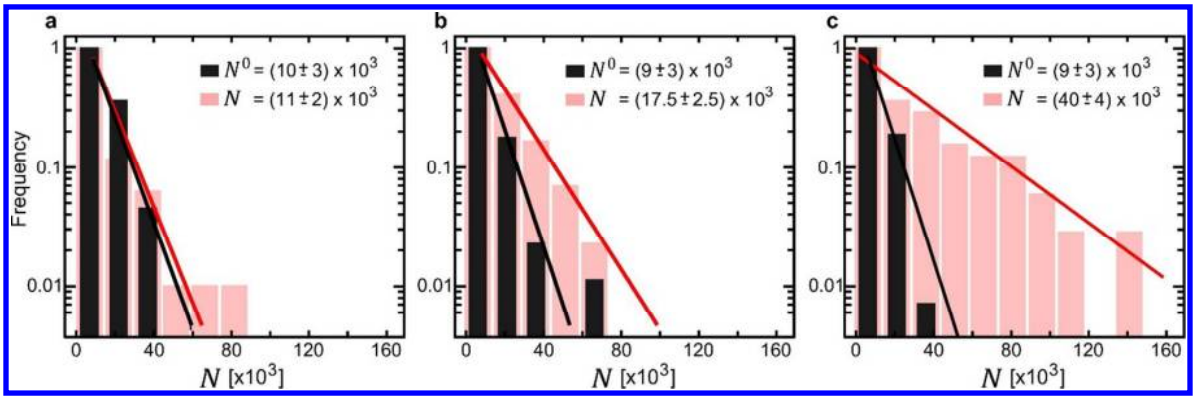

Figure 3. Normalized frequency histograms of total number of detected photons N from the Cy5 molecules in the samples with AuNPs of 20 (a), 40 (b) and 80 nm (c). For each sample N is computed for the populations of DNA-Cy5 constructs without (reference, black) and with AuNPs attached (red). Each histogram is fitted with a single exponential (lines). The mean number of photons obtained from the decay constant ±2σ estimated from the fitting is shown in the legends.

Total number of photons before photobleaching

In contrast to the intensity, the total number of fluorescence photons emitted by a molecule does not depend on the excitation rate (equation 2). At this point it is important to note that photobleaching is a stochastic process, result of a single or a set of multiple photochemical reactions that leads to the average rate k_b. The number of total emitted photons by each individual fluorophore is a variable that follows an exponential distribution. Looking only at individual behaviors, e.g. the maximum number of photons emitted by one particular molecule, does not provide any meaningful information. In other words, even in the reference population, if enough molecules were measured, one molecule would be found, belonging to the asymptotic tail of the exponential distribution, that would emit an arbitrarily high number of photons way above the sample average.

Determining changes of photo-stability reliably requires the proper measurement of the distribution of total photons emitted by the fluorophores. For each single molecule transient, we computed the total number of photons detected until single-step photobleaching occurred (N). In figure 3, the distributions of N are shown for each population of fluorophores. The first observation is that all distributions are monoexponential confirming that each population selected by fluorescence lifetime presents a single k_r/k_b ratio. In all three samples the reference populations present an average number of about 9,000 total detected photons. The fluorophores in the constructs with the smaller AuNPs of 20 nm present a distribution that is statistically indistinguishable to the references, indicating that the observed reduction of fluorescence lifetime is essentially due to an increase of k_{nr}. As the AuNP diameter increases to 40 and 80 nm, the average number of detected photons increases to approximately 17,500 and 40,000; i.e. roughly a 1.9 and 4.3-fold increase in comparison to the free fluorophores, respectively. Based on equation (2) and the larger number of detected photons, the 40 and 80 nm AuNPs produce a noticeable increase in the molecular radiative decay rate k_r.

Theoretical modelling

A unique advantage of the DNA self-assembled constructs is the great geometrical precision they provide to fabricate nano-structures. In our case, the fluorophores are placed at controlled nanometric distances from the AuNPs which enables the accurate modelling of their optical response[32]. The AuNP is modelled as a sphere of the nominal nanoparticle size, made of gold. The fluorophore is modelled as a 1.5 nm (point-like) dipole oscillating at the frequency of 448 THz corresponding to the peak emission wavelength of the Cy5 dye (669 nm). Both the gold sphere and the point dipole are immersed in water. The response of the system is obtained by calculating the electromagnetic field with a 3D finite difference time domain (FDTD) software (Microwave Studio, Computer Simulation Technology, Darmstadt, Germany).

The variations of k_r produced by the AuNPs are calculated as follows:

$$k_r/k_r^0 = \frac{\iint P(\varphi,\theta)d\Omega}{\iint P_0(\varphi,\theta)d\Omega}$$

Where $P(\varphi,\theta)$ and $P_0(\varphi,\theta)$ are the angular emitted power for the AuNP-dipole system and for the reference situation of the same dipole emitter in water, respectively. The angles φ and θ are the usual azimuthal and polar angles in spherical coordinates and the integration is performed over full space. Naturally, only the ratio of calculated emitted powers is meaningful to compare to experimental variation of k_r in the absence and presence of the AuNP. The actual values of $\iint P d\Omega$ and $\iint P_0 d\Omega$ depend on the strength of the dipolar emitter (i.e. in the simulations, size and current) just as the actual value of k_r depends on the fluorophore used. The ratio k_r/k_r^0 was calculated for various diameters of the gold sphere for dipoles oriented along the tangential and radial directions with respect to the sphere (figure 4). The experimental situation of randomly oriented fluorophores is approximated by an average of 2/3 tangential dipoles and 1/3 of radially oriented dipoles. In order to test the validity of the steady state bleaching model, the variation of k_r must be contrasted to the relative variation of the number of total detected photons N/N^0 (where N and N^0 denote the number of detected photons in the presence and absence of the AuNP). In figure 4, we plotted the experimental values of N/N^0 together with the calculated values of k_r/k_r^0. The excellent agreement between calculations and experimental results is clearly evident, confirming that the improved photostability is a consequence of an enhancement of k_r.

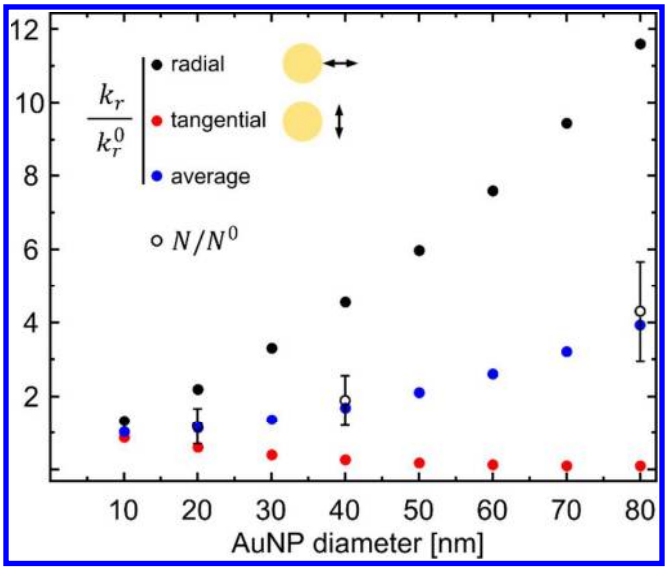

Figure 4. Calculated variation of the molecular radiative decay rate (k_r/k_r^0) and experimental change in the number of detected photons (N/N^0), relative to the situation without AuNP, as a function of the diameter of the AuNP. The calculations were carried out for different dipole orientations as indicated. The average, representing the experimental situation of randomly oriented dipoles with respect to the AuNP, is represented by 2/3 of the tangential k_r and 1/3 of the radial k_r. Error bars represent the propagation of ±2σ estimated error from the fitting of the distributions of N (figure 2).

For all AuNP sizes, the observed fluorescence lifetime was of about 100 ps, limited by the duration of the laser pulses used. Although a quantitative discussion is not possible because the lifetime measurements were limited by the instrument response, one can set a minimum reduction in lifetime of about 10 times. Since the change in k_r produced by the 20 nm AuNP is negligible, the (at least) 10-fold decrease in lifetime should be an exclusive consequence of a strong increase of k_{nr}. Local enhancement of the excitation field should account for the fact that the fluorescence intensity is reduced only about 3 times, and not 10 times or more. The increment in k_r by a factor of 1.9 and 4.3, produced by the 40 and 80 nm AuNP, respectively, is also insufficient to account for the 10-fold lifetime reduction, indicating that k_{nr} has increased even more than k_r. Despite the reduced quantum efficiency, the detected signals are not reduced and even enhanced for the 80 nm AuNP due to a strong enhancement of the excitation field[28].

Conclusions

We demonstrated that the total number of fluorescence photons detected from a fluorophore before photobleaching can be controlled by electromagnetic coupling to a metallic nanoparticle in the near field. For fluorophores placed at 8.5 nm from the AuNP surface, the increase in photostability is found to depend strongly on the AuNP size. AuNPs of 20 nm produced a negligible effect, whereas the 80 nm AuNP made the fluorophores to emit more than four times more photons before photobleaching.

DNA self-assembly is an excellent strategy to produce large amounts of nano-sized hybrid constructs containing fluorophores and metallic nanoparticles in a well-defined geometry. This unmatched precision in the geometrical structuring enables the accurate theoretical modelling. Comparison of the experimental results to the theory demonstrates that the number of total emitted photons before photobleaching is proportional to the changes of the radiative decay rate of the fluorophores. Confirmation of this mechanism establishes a clear guideline for the exploration of new schemes and hybrid nano-structures able to manipulate photostability of fluorophores and other photochemical reactions. Also, it provides a way to determine changes in the radiative rate of fluorophores, which in combination with lifetime measurements gives access to all photophysical rates of the fluorescence process. The radiative rate of fluorophores in close proximity to metallic nanoparticles can be enhanced much more than in the present experiments by optimizing distances and resonance conditions. Remarkably, as the non-radiative rate does not affect the number of emitted photons, even in situations of strong quenching one should be able to harvest orders of magnitude more fluorescence photons before photobleaching.

Materials and Methods

Sample preparation. Nanoparticles are functionalized with a T_{15}- DNA strand with a thiol modification on the 5'-end according to ref.[33]. The DNA origami structures are folded as described previously[28], a list of the single "staple" strands is included on the Supporting Information. The DNA origami are filtered three times with a buffer containing 1xTAE and 12.5 mM $MgCl_2$ (Amicon Ultra-0.5 ml Centrifugal Filters, 100,000 MWCO) at 14,000 rcf for 8 minutes and then recovered for 2 minutes at 1,000 rcf. Immobilization was carried out on BSA/BSA-biotin/neutravidin surfaces as shown in ref[28] in 1xPBS with 12.5 mM $MgCl_2$. After the DNA origamis are bound we incubate the sample with a buffer containing 1xPBS, 700 mM NaCl and the gold NPs of the different sizes until a sufficient fraction of DNA origami is equipped with a NP. The final measurement buffer consists of 1x PBS.

Time resolved single-molecule measurements. Single-molecule fluorescence transients are measured with a custom built confocal setup based on an inverted microscope (IX71, Olympus) with a high NA oil immersion objective (100x/NA 1.40, UPLSAPO100XO). The Cy5 dye molecules are excited at 640 nm with an 80 MHz pulsed laser diode (LDH-D-C-640, Picoquant) delivering 1 µW at the objective pupil. A combination of linear polarizer and quarter wave plate ensures circular

polarization of the laser beam which is guided to the sample by a dichroic beamsplitter (Dualband z532/633, AHF). The surface with immobilized DNA origamis is imaged by scanning the sample with a piezo stage (P-517.3CL, Physik Instrumente). From that image, molecules are selected and placed in the laser focus for time resolved analysis. The resulting fluorescence is collected by the same objective and separated from the excitation light after focusing on a 50 µm pinhole by two filters (Bandpass ET 700/75m, AHF; RazorEdge LP 647, Semrock). The signal is detected by a single photon counting module (τ-SPAD 100, Picoquant) and a PC-card for time-correlated single-photon counting (SPC-830, Becker&Hickl). The raw data is processed with custom made software (LabView2009, National Instruments).

Fluorescence lifetime analysis. The fluorescence lifetime decays were fitted with a mono-exponential function convoluted with the experimental instrument response function using a custom routine written in IgorPro (Wavemetrics, inc.).

Acknowledgements

We are grateful to Frank Demming for assistance with the numerical simulations. This work was carried out at the NanoBioScience group, Braunschweig University of Technology and was supported by a starting grant (SiMBA, EU 261162) of the European Research Council (ERC). TU Braunschweig, G. P. A. and P. T. have filed a provisional patent application, EP1260316.1., on the described method of creating hotspots using self-assembled DNA origami. We are grateful to the DAAD for the exchange fellowship for J.V.P. and to the ANCyPT for financial support (PICT2010-2511).

References

(1) Hirschfeld, T. *Appl. Opt.* **1976**, *15*, 3135–3139.

(2) Panchuk-Voloshina, N.; Haugland, R. P.; Bishop-Stewart, J.; Bhalgat, M. K.; Millard, P. J.; Mao, F.; Leung, W.-Y. *J. Histochem. Cytochem.* **1999**, *47*, 1179–1188.

(3) Avlasevich, Y.; Li, C.; Müllen, K. *J. Mater. Chem.* **2010**, *20*, 3814.

(4) Altman, R. B.; Terry, D. S.; Zhou, Z.; Zheng, Q.; Geggier, P.; Kolster, R. a; Zhao, Y.; Javitch, J. a; Warren, J. D.; Blanchard, S. C. *Nat. Methods* **2012**, *9*, 68–71.

(5) Rasnik, I.; McKinney, S. A.; Ha, T. *Nat. Methods* **2006**, *3*, 891–893.

(6) Benesch, R. E.; Benesch, R. *Science (80-.).* **1953**, *118*.

(7) Yildiz, A.; Tomishige, M.; Vale, R. D.; Selvin, P. R. *Science (80-.).* **2004**, *303*, 676–678.

(8) Vogelsang, J.; Kasper, R.; Steinhauer, C.; Person, B.; Heilemann, M.; Sauer, M.; Tinnefeld, P. *Angew. Chemie* **2008**, *47*, 5465–5469.

(9) Ha, T.; Tinnefeld, P. *Annu. Rev. Phys. Chem.* **2012**, *63*, 595–617.

(10) Purcell, E. *Phys. Rev.* **1946**, *69*, 681.

(11) Drexhage, K. H. *Prog. Opt.* **1974**, *12*, 163–232.

(12) Chance, R.; Prock, A.; Silbey, R. *Adv. Chem. Phys.* **1978**, *37*, 1.

(13) Barnes, W. L. *J. Mod. Opt.* **1998**, *45*, 661–699.

(14) Novotny, L.; Hecht, B. *Principles of Nano Optics*; First edit.; Cambridge University Press, 2006.

(15) Lakowicz, J. R. *Anal. Chem.* **2005**, *337*, 171–194.

(16) Stefani, F. D.; Vasilev, K.; Bocchio, N.; Gaul, F.; Pomozzi, A.; Kreiter, M. *New J. Phys.* **2007**, *9*, 21–21.

(17) Hoogenboom, J. P.; Sanchez-Mosteiro, G.; Colas des Francs, G.; Heinis, D.; Legay, G.; Dereux, A.; van Hulst, N. F. *Nano Lett.* **2009**, *9*, 1189–1195.

(18) Kühn, S.; Håkanson, U.; Rogobete, L.; Sandoghdar, V. *Phys. Rev. Lett.* **2006**, *97*, 017402.

(19) Muskens, O. L.; Sanchez-Gil, J. A.; Giannini, V.; Gomez-Rivas, J. *Nano Lett.* **2007**, *7*, 2871–2875.

(20) Busson, M. P.; Rolly, B.; Stout, B.; Bonod, N.; Bidault, S. *Nat. Commun.* **2012**, *3*, 962.

(21) Enderlein, J. *Chem. Phys.* **1999**, *247*, 1–9.

(22) Malicka, J.; Gryczynski, I.; Fang, J.; Kusba, J.; Lakowicz, J. R. *J. Fluoresc.* **2002**, *12*, 439–447.

(23) Vasilev, K.; Stefani, F. D.; Jacobsen, V.; Knoll, W.; Kreiter, M. *J. Chem. Phys.* **2004**, *120*, 6701–6704.

(24) Zaiba, S.; Lerouge, F.; Gabudean, A.-M.; Focsan, M.; Lermé, J.; Gallavardin, T.; Maury, O.; Andraud, C.; Parola, S.; Baldeck, P. L.; Lerm, J. *Nano Lett.* **2011**, *11*, 2043–2047.

(25) Cang, H.; Liu, Y.; Wang, Y.; Yin, X.; Zhang, X. *Nano Lett.* **2013**, *13*, 5949–5953.

(26) Rothemund, P. W. K. *Nature* **2006**, *440*, 297–302.

(27) Möller, F. M.; Holzmeister, P.; Sen, T.; Acuna, G. P.; Tinnefeld, P. *Nanophotonics* **2013**, *2*, 167–172.

(28) Acuna, G. P.; Möller, F. M.; Holzmeister, P.; Beater, S.; Lalkens, B.; Tinnefeld, P.; Moller, F. M. *Science (80-.).* **2012**, *338*, 506–510.

(29) Coronado, E. a; Encina, E. R.; Stefani, F. D. *Nanoscale* **2011**, *3*, 4042–4059.

(30) Schmied, J. J.; Forthmann, C.; Pibiri, E.; Lalkens, B.; Nickels, P.; Liedl, T.; Tinnefeld, P. *Nano Lett.* **2013**, *13*, 781–785.

(31) Yu, X.; Lei, D. Y.; Amin, F.; Hartmann, R.; Acuna, G. P.; Guerrero-Martínez, A.; Maier, S. a.; Tinnefeld, P.; Carregal-Romero, S.; Parak, W. J. *Nano Today* **2013**, *8*, 480–493.

(32) Acuna, G. P.; Bucher, M.; Stein, I. H.; Steinhauer, C.; Kuzyk, A.; Holzmeister, P.; Schreiber, R.; Moroz, A.; Stefani, F. D.; Liedl, T.; Simmel, F. C.; Tinnefeld, P. *ACS Nano* **2012**, *6*, 3189–3195.

(33) Mirkin, C.; Letsinger, R.; Mucic, R.; Storhoff, J. *Nature* **1996**, *382*, 607–609.

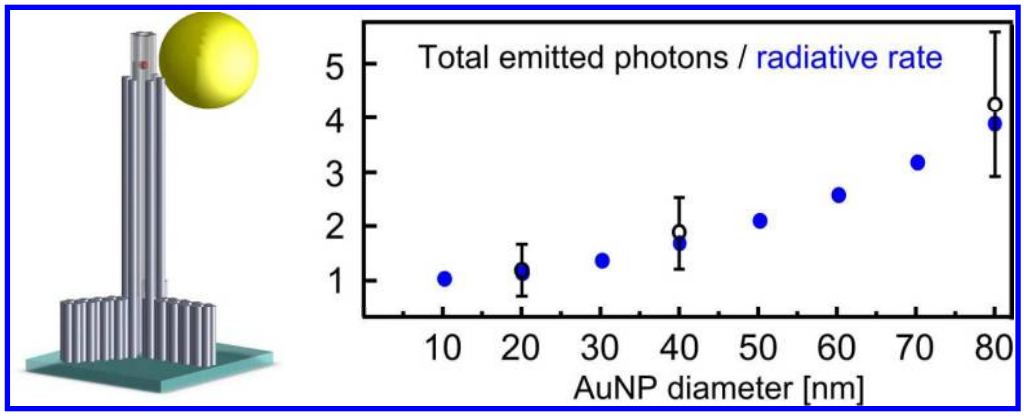

For TOC Only
727x285mm (72 x 72 DPI)